

Circ_0010235 Regulates HOXA10 Expression to Promote Malignant Phenotypes and Radioresistance in Non-small Cell Lung Cancer Cells Via Decoying miR-588

Hongyan Zhu^{1#}, Wenshu Yang^{2#}, Qingping Cheng², Shuai Yang²

¹Oncology Xiangyang No.1 People's Hospital, Hubei University of Medicine, Hubei, China

²Respiratory and Critical Care Medicine Xiangyang Central Hospital, Affiliated Hospital of Hubei University of Arts and Science, Hubei, China

#Contributed equally

Background: Circular RNAs (circRNAs) are key modulators in carcinogenesis and radioresistance in multiple kinds of human cancers.

Aims: To explore the role of circ_0010235 in non-small cell lung cancer (NSCLC).

Study Design: Cell culture study and animal study.

Methods: The detection of circ_0010235, microRNA-588 (miR-588), and homeobox protein A10 (HOXA10) was implemented via reverse transcription-quantitative polymerase chain reaction (RT-qPCR). CCK-8, EdU, flow cytometry, transwell, and wound healing assays. These strategies were applied to evaluate cell functions. The western blot technique was employed for protein examination. The colony formation assay was used to determine cell survival after radiation treatment. In vivo research was performed by tumor xenograft assay. The binding analysis was also carried out through dual-luciferase reporter and RNA immunoprecipitation studies.

Results: Circ_0010235 had an enhanced expression in NSCLC.

Circ_0010235 deficiency inhibited cell proliferation, invasiveness, and migratory ability but promoted apoptosis and radiosensitivity. Downregulation of circ_0010235 decelerated tumor growth and promoted radiation sensitivity in vivo. Circ_0010235 was controlled biologically in NSCLC cells by combining with miR-588 and targeting miR-588. HOXA10 acted as a target of miR-588. MiR-588 upregulation inhibited NSCLC cell malignant phenotypes and elevated radiosensitivity via downregulating HOXA10. Circ_0010235 could regulate the level of HOXA10 by sponging miR-588.

Conclusion: Circ_0010235 contributed to the malignant progression of NSCLC, but suppressed the radiation sensitivity via targeting miR-588 to induce HOXA10 upregulation.

INTRODUCTION

Non-small cell lung cancer (NSCLC) is one of the most common cancer types with the highest cancer-related mortality rates.¹ The early detection system of NSCLC is ineffective and the majority of patients progress to advanced stages.² In addition, tumor metastasis and radiation resistance are pivotal causes of poor survival and therapeutic failure in NSCLC patients.³ Thus, it is essential to investigate the contributing pathogenic mechanisms behind NSCLC to uncover novel strategies for effective treatment.

Circular RNAs (circRNAs) are closed-loop noncoding RNAs (ncRNAs) with important implications for the occurrence and progression of NSCLC.⁴ MicroRNAs (miRNAs) are small endogenous ncRNAs that play a major role in cancer initiation and

progression, including NSCLC.⁵ More interestingly, circRNAs are associated with gene-level regulation via interacting with miRNAs to function as “miRNA sponges” in human cancers.⁶ Circ_0010235 was reported to drive the progression of NSCLC by targeting the miR-433-3p/TIPRL axis and miR-338-3p/KIF2A axis.^{7,8} This further attests to the vital roles and special mechanisms of circ_0010235 in NSCLC development. However, the extensive role of circ_0010235 in NSCLC in terms of radioresistance has not been reported. This stems from the fact that its regulatory mechanisms remain not fully understood.

With regards to the molecular sponge effect of circ_0010235 on target microRNAs (miRNAs), the bioinformatics tool displays the computational binding site between circ_0010235 and miR-

Corresponding author: Shuai Yang, Respiratory and Critical Care Medicine Xiangyang Central Hospital, Affiliated Hospital of Hubei University of Arts and Science, Hubei, China

e-mail: hukeke0702@163.com

Received: February 12, 2022 Accepted: June 02, 2022 Available Online Date: July 22 • DOI: 10.4274/balkanmedj.galenos.2022.2022-2-50

Available at www.balkanmedicaljournal.org

ORCID iDs of the authors: H.Z. 0000-0001-7601-9080; W.Y. 0000-0001-9858-0477; Q.C. 0000-0002-1600-1345; S.Y. 0000-0003-4582-7231.

Cite this article as:

Zhu H, Yang W, Cheng Q, Yang S. Circ_0010235 Regulates HOXA10 Expression to Promote Malignant Phenotypes and Radioresistance in Non-small Cell Lung Cancer Cells Via Decoying miR-588. *Balkan Med J*; 2022; 39(4):255-266.

Copyright@Author(s) - Available online at <http://balkanmedicaljournal.org/>



588. Qian et al.⁹ demonstrated that miR-588 restrained the migration and invasion of lung carcinoma cells. It is unclear whether circ_0010235 exerts the sponge effects on miR-588 in NSCLC. Homeobox protein A10 (HOXA10) is a well-known oncogene in human cancers, including gastric cancer, colorectal cancer, and bladder cancer.¹⁰⁻¹² Also, HOXA10 was associated with tumor-promoting activity in NSCLC.^{13,14} Moreover, long ncRNAs inhibited radiosensitivity in lung adenocarcinoma via the upregulation of HOXA10 by binding to miRNAs.^{15,16} The relationships among circ_0010235, miR-588, and HOXA10 in NSCLC regulation are yet to be determined.

This study focused on the potential of circ_0010235, as a miR-588 sponge, to affect the expression level of HOXA10 in NSCLC. Meanwhile, the role of circ_0010235 in regulating radiosensitivity was investigated in NSCLC cells and murine models. A novel circRNA/miRNA/mRNA axis was established to disclose the carcinogenesis and radiosensitivity of NSCLC.

MATERIALS AND METHODS

Tissue Specimens

This study included a total of 29 NSCLC patients from Xiangyang No.1 People's Hospital. Tumor tissues (n = 29) and normal controls (n = 29) were collected during the surgical resection, snap-frozen by liquid nitrogen, and conserved at -80 °C. The clinicopathologic features of patients with NSCLC and their association with circ_0010235 expression are contained in Table 1.

Cell Cultures and Transfections

NSCLC cells (H1650, A549, and H1299) and human bronchial endothelial cell lines (HBE) were acquired from BioVector NTCC Inc. (Beijing, China). The Dulbecco's modified eagle medium (DMEM; Gibco, Carlsbad, CA, USA) was pipetted with 10% fetal bovine serum (FBS, Gibco). The cells were cultured in a humidified incubator at 5% CO₂ and 37 °C; afterward, RNA or

plasmid transfection was performed using Lipofectamine™ 3000 Kit (Invitrogen, Carlsbad, CA, USA) in A549 and H1299 cells. RNAs were purchased from GenePharma (Shanghai, China), including small interfering RNAs (si-circ_0010235 and si-NC), mimics (miR-588 and miR-NC), and inhibitors (anti-miR-588 and anti-miR-NC). The short hairpin RNA lentiviral vectors (sh-circ_0010235 and sh-NC) were provided by RIBOBIO (Guangzhou, China). The pcDNA expression vector (GENESEED, Guangzhou, China) was cloned with the HOXA10 sequence to construct the pcDNA-HOXA10 overexpression vector.

Reverse Transcription-quantitative Polymerase Chain Reaction (RT-qPCR) Assay

Total RNA was extracted from tissue samples and cell lysates using the Beyozol reagent (Beyotime, Shanghai, China). BeyoRT™ III First Strand cDNA Synthesis Kit (Beyotime) was used for the reverse transcription assay. BeyoFast™ SYBR Green qPCR Mix Kit (Beyotime) was used for PCR detection. The relative expression level of each gene was calculated using the 2^{-ΔΔCt} technique.¹⁷ Glyceraldehyde-phosphate dehydrogenase (GAPDH) for circ_0010235 or HOXA10 and U6 for miR-588 served as the internal controls. For analysis of stability, circ_0010235 and ALDH4A1 levels were determined by RT-qPCR after total RNA was performed with the treatment of RNase R (GENESEED). Reverse transcription using random or oligo (dT)₁₈ primers were used to identify the circular structure, followed by expression quantification of circ_0010235 and ALDH4A1. Table 2 shows the primer sequences.

Cell Viability Assay

CCK-8 cell viability analysis was done according to the instruction of Invitrogen. In brief, 10 μl/well CCK-8 reagent was added to react with cells for 3 hours, following the different cell transfections. The optical density was detected at a wavelength of 450 nm using a microplate reader (Thermo Fisher Scientific, Waltham, MA, USA).

TABLE 1. Relationship Between circ_0010235 Expression and Clinicopathologic Features of Patients with Non-small Cell Lung Cancer

Characteristics n = 29	circ_0010235 expression		P value
	Low (n = 14)	High (n = 15)	
Age (years)			0.7152
≤50	15	8	
>50	14	6	
TNM grade			0.0253*
I+II	12	9	
III	17	5	
Lymph node metastasis			0.0209*
Positive	19	6	
Negative	10	8	
Tumor size			0.0092*
≤3 cm	13	10	
>3 cm	16	4	

TNM, tumor-node-metas-tasis; *P < 0.05

Cell Proliferation Assay

4×10^4 cells were seeded in 48-well plates, which were then transfected. The proliferation of the cells was monitored using EdU Cell Proliferation Kit (Sigma, St. Louis, MO, USA). In addition, the cell nucleus was stained using a DAPI staining solution (Beyotime). EdU-positive cells were identified as those cells merged by EdU and DAPI. Cell images were obtained by fluorescence microscopy (Olympus, Tokyo, Japan).

Cell Apoptosis Assay

3×10^4 cells were harvested and suspended in 1x Binding Buffer; afterward, cell staining was performed with Annexin V-fluorescein isothiocyanate (Annexin V-FITC) and propidium iodide (PI) using the Annexin V Apoptosis Detection Kit (Beyotime). A flow cytometer (BD Biosciences, San Diego, CA, USA) was used for cell observation and analysis. The rate of apoptosis was measured as the percentage of (Annexin V+/PI- and Annexin V+/PI+)-stained cells.

Cell Invasion Assay

The transwell chamber (Corning Inc., Corning, NY, USA) was coated with matrigel (Corning Inc.) and seeded with 1×10^5 cells in the upper chamber and 10% FBS+DMEM medium in the lower chamber. After incubation for 24 hours, the invaded cells were stained with 0.1% crystal violet (Sigma) and photographed with an inverted microscope (Olympus). Cell images were obtained at $100 \times$ magnification and cells were counted under the five fields of view.

Cell Migration Assay

Twelve-well plates were inoculated with 2×10^5 transfected A549 and H1299 cells, followed by the production of two straight scratches through a sterile 200 μ L pipette tip. 200 μ L of phosphate buffer solution (PBS; Gibco) was added to remove the waste cells. The plates were then incubated with DMEM medium without FBS. The wound width was determined at 0 and 24 hours. The migration distance was expressed as the wound width_(0 h) - wound width_(24 h).

TABLE 2. Primer Sequences used for RT-qPCR

Name	Primer sequences (5'-3')
circ_0003528	Forward: GTAACCAGCAGCCTGGACTC Reverse: GCAACTTGCTGACCAGAACAA
miR-1252-5p	Forward: GTATGAAGAAGGAAATTGAAT Reverse: CTCAACTGGTGTGCGTGGAG
HOXA10	Forward: CTGGTTTCAGAACCGCAGGA Reverse: AGATGTAACGGCCAGGAGA
ALDH4A1	Forward: CGCTTCTAACCGAGATGCT Reverse: GGTCTTCAAGGCCTTTGC
GAPDH	Forward: AAGGCTGTGGCAAGGTCATC Reverse: GCGTCAAAGGTGGAGGAGTGG
U6	Forward: CTCGCTTCGGCACACATA Reverse: CGAATTGCGTGTACATCCT

Western Blotting Analysis

Western blotting was performed for protein-level analysis in tissues and cells. Total proteins were obtained by the radioimmunoprecipitation assay (Thermo Fisher Scientific) and quantified using the BCA Protein Quantification Kit (Thermo Fisher Scientific). Subsequently, 40 μ g of proteins were loaded on 10% Bis-Tris gels (Invitrogen) and transferred onto polyvinylidene fluoride membranes (Thermo Fisher Scientific). The primary antibodies for c-myc (CST, Boston, MA, USA, #18583, 1:1000), cleaved-caspase-3 (CST, #9661, 1:1000), HOXA10 (CST, #58891, 1:1000), and GAPDH (CST, #8884, 1:1000) were incubated at 4 °C overnight. The membranes were then incubated with the Anti-rabbit IgG secondary antibody (#7054) at room temperature for 45 min, followed by visualization of protein bands using Pierce™ ECL Plus Western Blotting Substrate (Thermo Fisher Scientific). The images showing the protein expression level were quantified using the ImageJ software (NIH, Bethesda, MD, USA).

Radiosensitivity Assay

A549 and H1299 cells were plated into the 6-well plates at 5×10^4 and transfected cells were treated with increasing doses of x-ray radiation (0 Gy, 2 Gy, 4 Gy, 6 Gy, and 8 Gy) using X-ray linear accelerator (Siemens, Concord, CA, USA). The radiation rate was 2 Gy/min; afterward, the cells were cultured at 37 °C for 12 days, and colonies were dyed with 0.1% crystal violet (Sigma). The survival fraction was calculated using the formula: (colony number/plating number) of the radiation group/(colony number/plating number) of the control group.

In Vivo Experiments

H1299 cells were infected with the sh-circ_0010235 lentiviral vector using the sh-NC vector as the negative control. 24 male BALB/c nude mice (Vital River, Beijing, China) were assigned into four groups (sh-NC, sh-NC+IR, sh-circ_0010235, sh-circ_0010235+IR) with six mice per group. Transfected H1299 cells (2×10^6) were injected into the rank of back in mice, followed by 4 Gy irradiation every week. Eight days later, the tumor volume (length × width²/2) was calculated every four days. Mice were sacrificed according to the current guideline of the American Veterinary Medical Association (AVMA) at 28 days, after which the tumors were dissected and weighed. Total RNA was extracted for the detection of circ_0010235 level using RT-qPCR. In addition, the immunohistochemical (IHC) assay was implemented to measure the protein levels of Ki67 (Abcam, Cambridge, UK, ab15580) and C-myc (Abcam, ab32072) in tissues. This xenograft tumor assay was ratified by the Animal Ethical Committee of Xiangyang No.1 People's Hospital.

Dual-luciferase Analysis

The target binding sites were predicted using starbase (<http://starbase.sysu.edu.cn>). The circ_0010235 and HOXA10 sequences were cloned into the pmirGLO plasmid (Promega, Madison, WI, USA) to construct the wild-type (WT, containing the complementary sites of miR-588) plasmids WT-circ_0010235

and WT-HOXA10 3'UTR or the mutant-type (MUT, containing the mutated sites of miR-588) plasmids MUT-circ_0010235 and MUT-HOXA10 3'UTR. Luciferase activity was instantly examined using the Dual-luciferase Reporter Detection Kit (Promega) after co-transfection with each plasmid and miR-588 or miR-NC for 48 h.

RNA Immunoprecipitation (RIP) Assay

The binding relation between miR-588 and circ_0010235 or HOXA10 was analyzed through the Imprint® RNA Immunoprecipitation Kit (Sigma). The magnetic beads were coated with immunoglobulin G (IgG) antibody or Argonaute-2 (Ago2) antibody, followed by incubation with lysates of A549 and H1299 cells at 4 °C overnight. The RNA complexes were isolated from the beads and the expressions of circ_0010235, miR-588, and HOXA10 were quantified by RT-qPCR.

Statistical Analysis

All experiments were conducted in triplicates. Data were expressed as the mean ± standard deviation and analyzed by IBM SPSS Statistics for Windows, version 22 (IBM Corp., Armonk, N.Y., USA). For the linear analysis, Pearson's correlation was performed for the human NSCLC tissues. The student's t-test or analysis of variance, followed by Tukey's post hoc test, was employed to determine statistical differences at $P < 0.05$.

RESULTS

Circ_0010235 was Highly Expressed in NSCLC Samples and Cells

A total of 29 pairs of normal and tumorigenic tissues were utilized in this study. Subsequently, we determined the level of circ_0010235 in the tissue samples. As shown in Figure 1a, circ_0010235 was significantly overexpressed in NSCLC tissues relative to normal tissues. Meanwhile, a high expression of circ_0010235 was observed in NSCLC cell lines (H1650, A549, and H1299), in contrast to the normal HBE cell line (Figure 1b). Thus, A549 and H1299 cells were selected for further research. The linear expression of ALDH4A1 was inhibited in the RNase R group in contrast with the Mock group; however, circ_0010235 was not affected by the RNase R treatment (Figure 1c and 1d). Thus, circ_0010235 was more stable than its linear transcript in NSCLC cells. Given that oligo (dT)₁₈ primers can combine with the 3'-polyA tails of linear RNA molecules, we used random primers or oligo (dT)₁₈ primers to testify to the circularity of circ_0010235. The results of RT-qPCR revealed that there was no difference in the ALDH4A1 level between the Random and Oligo (dT)₁₈ groups, whereas the expression of circ_0010235 was decreased in the Oligo (dT)₁₈ group (Figure 1e and 1f), suggesting that circ_0010235 was a circRNA without 3'-polyA tail. Overall, circ_0010235 was found to be abnormally overexpressed in NSCLC.

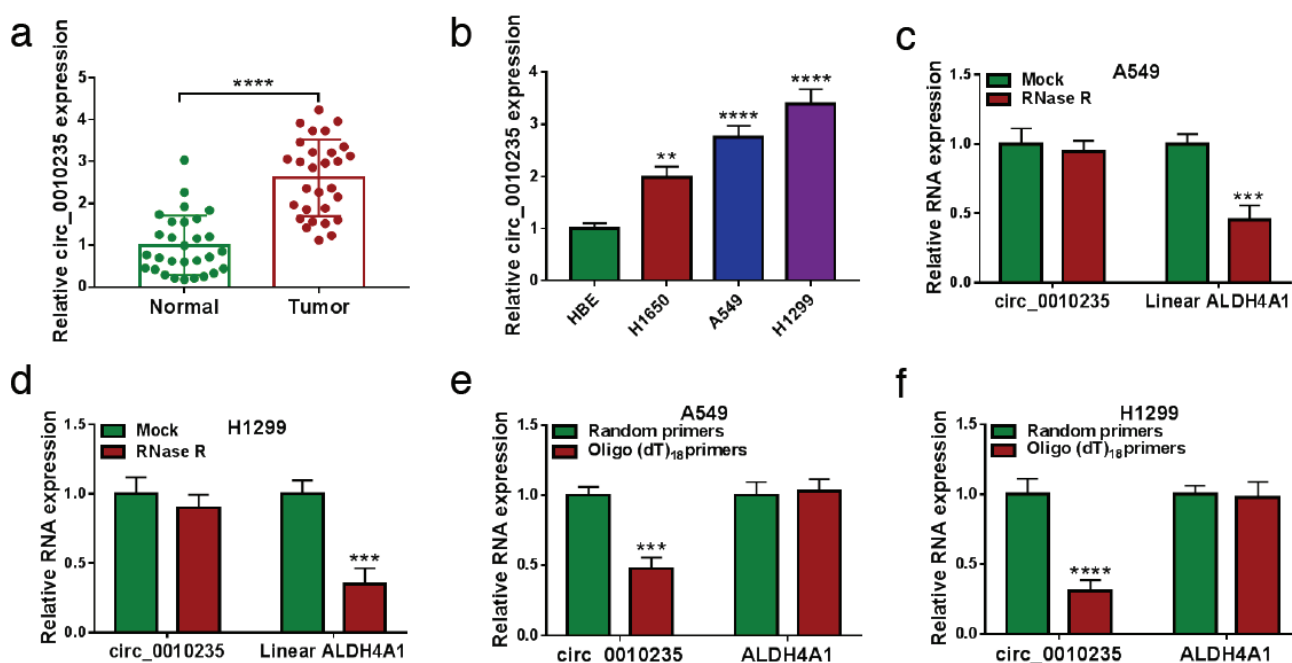


FIG. 1. Circ_0010235 was highly expressed in NSCLC tissues and cells. The expression of circ_0010235 was determined by RT-qPCR in NSCLC tissues (a) and cells (b). (c-d) Circ_0010235 and ALDH4A1 levels were examined by RT-qPCR after RNase R treatment in total RNA from A549 and H1299 cells. (e-f) The detection of circ_0010235 and ALDH4A1 expression was performed by RT-qPCR after reverse transcription using Random primers or Oligo (dT)₁₈ primers. ** $P < 0.01$, *** $P < 0.001$, **** $P < 0.0001$.

Circ_0010235 Downregulation Inhibits Malignant Behaviors and Increases Radiation Sensitivity in NSCLC Cells

The experimental cells were transfected with si-circ_0010235 and si-NC, respectively. RT-qPCR analysis revealed that circ_0010235 expression was downregulated in the si-circ_0010235 (#1, #2, and #3) groups compared to the si-NC group and that si-circ_0010235#3 showed the highest efficiency to deplete si-circ_0010235 expression (Figure 2a). Thus, si-circ_0010235#3, shortly written as si-circ_0010235, was utilized in the subsequent assays. CCK-8 and EdU assays showed that cell viability (Figure 2b) and proliferation (Figure 2c) were repressed after the silence of circ_0010235. Through flow cytometry, it was found that the downregulation of circ_0010235 induced apoptosis in A549 and H1299 cells (Figure 2d). The results indicate that circ_0010235 knockdown resulted in the suppression of cell invasion (Figure 2e) and migration (Figure 2f). Furthermore, protein detection by western blotting revealed

that the oncogene *c-myc* was downregulated and that cleaved-caspase-3 was highly expressed by the inhibition of circ_0010235 (Figure 2g and 2h). The colony formation assay revealed that cell survival was reduced after transfection of si-NC in radiation-exposed A549 and H1299 cells (Figure 2i and 2j). Taken together, the silencing of circ_0010235 impeded cancer progression and enhanced radiation sensitivity in NSCLC cells.

Knockdown of Circ_0010235 Suppresses Tumor Growth and Elevates Radiation Sensitivity In Vivo

RT-qPCR confirmed that circ_0010235 was markedly downregulated in sh-circ_0010235-transfected H1299 cells relative to sh-NC-transfected cells (Figure 3a). The tumors were monitored after cell injection and radiation treatment. The tumor volumes and weights were reduced by the downregulation of circ_0010235. In addition, the tumor growth was further inhibited in the sh-circ_0010235+IR group compared with the sh-NC+IR

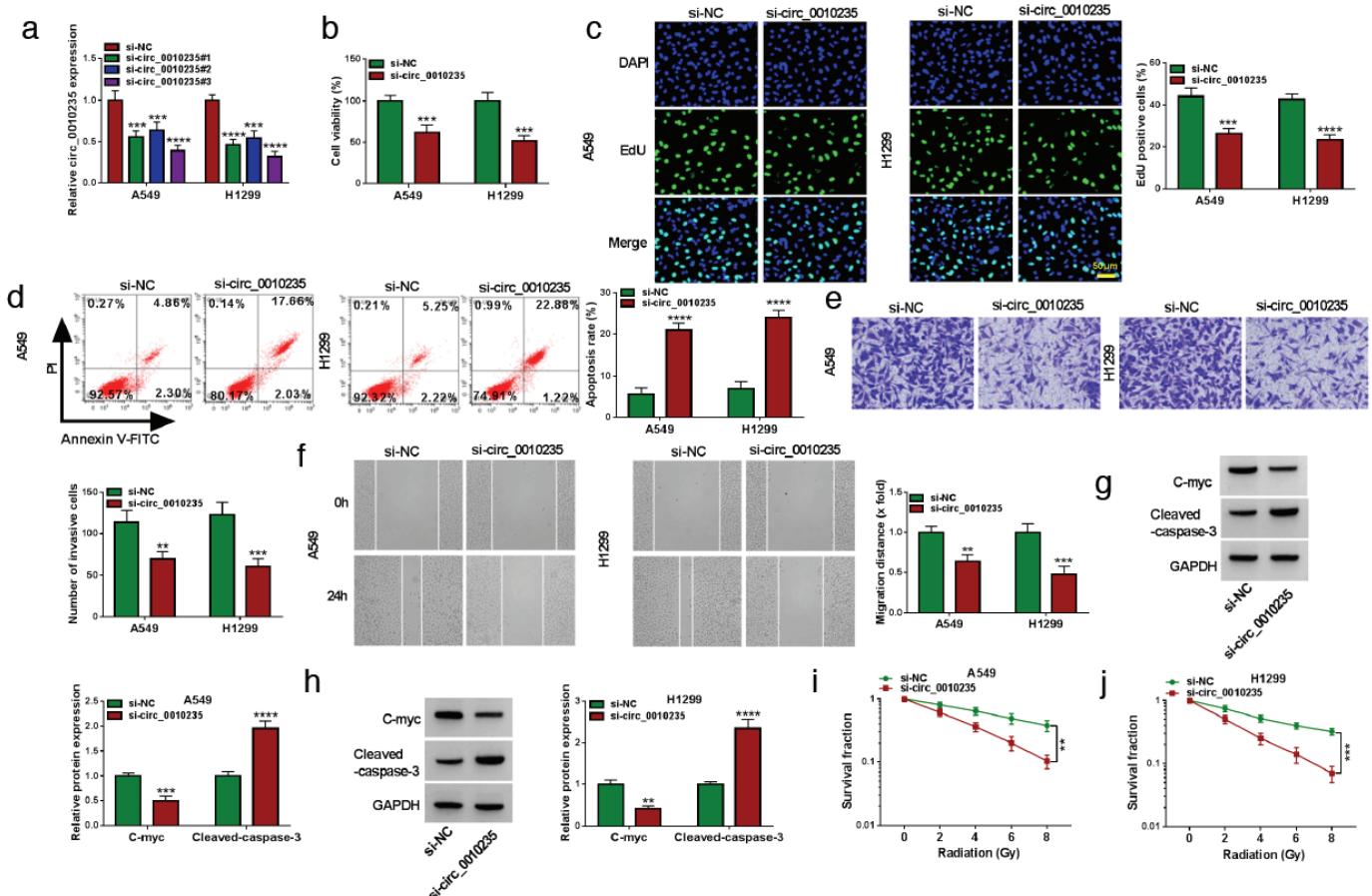


FIG. 2. Circ_0010235 downregulation inhibits malignant behaviors and increases radiation sensitivity in NSCLC cells. Transfection of si-NC or si-circ_0010235 was performed in A549 and H1299 cells. (a) The efficiency of circ_0010235#1, circ_0010235#2, and circ_0010235#3 were quantified using RT-qPCR to attenuate the off-target effect. (B-C) Cell viability (b) and proliferation (c) were analyzed using the CCK-8 and EdU assays, respectively. (d) Cell apoptosis was measured by flow cytometry. (e-f) Cell invasion (e) and migration (f) were evaluated using the transwell and wound healing assays, respectively. (g-h) C-myc and cleaved-caspase-3 protein levels were detected by western blotting. (i-j) Cell survival was assessed by colony formation assay after radiation exposure. ** $P < 0.01$, *** $P < 0.001$, **** $P < 0.0001$.

group (Figure 3b and 3c). Circ_0010235 level was lower in the sh-circ_0010235 and sh-circ_0010235+IR groups than in the sh-NC and sh-NC+IR groups (Figure 3d). The IHC assay showed that Ki67 and c-myc protein levels were inhibited by sh-circ_0010235 with or without radiation exposure (Figure 3e). Also, the knockdown of circ_0010235 repressed tumor growth and facilitated radiation sensitivity in the xenografts.

Circ_0010235 Interacts with miR-588

The starbase software predicted the miR-588 binding sites in the circ_0010235 sequence (Figure 4a). As a verification, the transfection of miR-588 notably enhanced the miR-588 level by comparison with the transfection of miR-NC, showing that miR-588 mimic evoked the high overexpression of miR-588 (Figure 4b). The upregulation of miR-588 induced the luciferase activity inhibition of the WT-circ_0010235 plasmid rather than the MUT-circ_0010235 plasmid, which suggests that circ_0010235 could combine with miR-588 in NSCLC cells (Figure 4c and 4d). Meanwhile, circ_0010235 and miR-588 were enriched by Ago2 in contrast with IgG (Figure 4e and 4f). The downregulation of miR-588 was detected in NSCLC tissues in contrast with normal controls (Figure 4g). Moreover, circ_0010235 expression was inversely related to miR-588 expression ($r = -0.8149$, $P < 0.001$)

in 29 tumor samples (Figure 4h). In comparison with normal HBE cells, the miR-588 level was reduced in A549 and H1299 cells (Figure 4i). These results reveal that circ_0010235 directly interacts with miR-588.

The Inhibition of miR-588 Counters the Regulatory Function of si-circ_0010235 in NSCLC Cells

The transfection of si-circ_0010235 upregulated the expression of miR-588, which was inhibited by anti-miR-588 (Figure 5a). With the inhibition of miR-588 expression, si-circ_0010235-mediated inhibitory effects on cell viability (Figure 5b) and proliferation (Figure 5c), as well as si-circ_0010235-mediated cell apoptosis (Figure 5d), were all relieved. Cell invasion and migration abilities were enhanced by co-transfection with si-circ_0010235 and anti-miR-588 relative to si-circ_0010235 transfection alone (Figure 5e and 5f). The si-circ_0010235-induced protein level changes of c-myc and cleaved-caspase-3 were abrogated by a miR-588 inhibitor in A549 and H1299 cells (Figure 5g and 5h). Moreover, anti-miR-588 transfection reversed si-circ_0010235-induced cell survival inhibition in A549 and H1299 cells exposed to radiation (Figure 5i and 5j). Taken together, circ_0010235 exerted oncogenic effects in NSCLC partly by inhibiting miR-588.

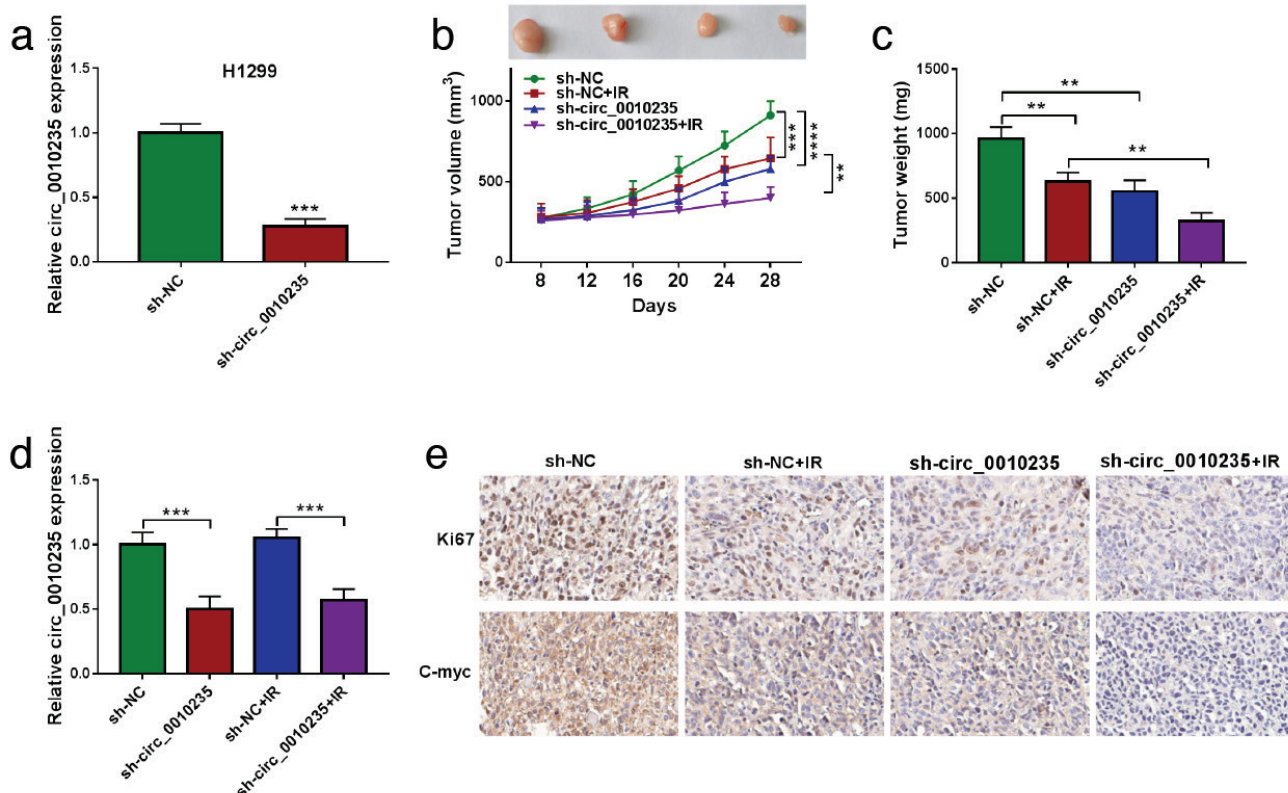


FIG. 3. Knockdown of circ_0010235 suppresses tumor growth and elevates radiation sensitivity in vivo. (a) The circ_0010235 level was measured via RT-qPCR after H1299 cells were transfected with sh-NC or sh-circ_0010235. (b-c) Tumor volume (b) and weight (c) were determined in the sh-NC, sh-NC+IR, sh-circ_0010235, and sh-circ_0010235+IR groups. (d) Circ_0010235 expression quantification was performed by RT-qPCR in the tissues of each group. (e) Ki67 and c-myc were detected by IHC analysis. ** $P < 0.01$, *** $P < 0.001$, **** $P < 0.0001$.

HOXA10 is a Downstream Target of miR-588

Target binding was predicted by starbase in HOXA10 3'UTR and miR-588 sequences (Figure 6a). The dual-luciferase (Figure 6b and 6c) and RIP assays (Figure 6d and 6e) confirmed that miR-588 binds to HOXA10 in A549 and H1299 cells. HOXA10 mRNA expression was higher in NSCLC tissues than in normal tissues (Figure 6f). There was a negative correlation ($r = -0.9127, P < 0.001$) between the expressions of miR-588 and HOXA10 mRNA (Figure 6g). Western blotting revealed that the HOXA10 protein level was elevated in the NSCLC samples (Figure 6h) and A549/H1299 cells (Figure 6i) in contrast to normal controls. The above data demonstrate that miR-588 targets the 3'UTR of HOXA10.

MiR-588 Acts as a Tumor Inhibitor and Radiation Sensitizer by Targeting HOXA10

HOXA10 protein level was reduced by miR-588 overexpression. This regulation by miR-588 was abrogated by the transfection of HOXA10 (Figure 7a). After miR-588 was upregulated, cell viability (Figure 7b) and proliferation (Figure 7c) were inhibited and apoptosis was enhanced (Figure 7d); however, these effects were attenuated by the introduction of HOXA10. The miR-588-induced cell invasion/migration inhibition (Figure 7e and 7f) and

c-myc downregulation/cleaved-caspase-3 upregulation (Figure 7g-h) were abrogated by the expression of HOXA10. In addition, cell survival was promoted in the miR-588+HOXA10 group compared to the miR-588+pcDNA group (Figure 7i and 7j). This confirms that miR-588 inhibited the progression and radiation sensitivity of NSCLC cells by targeting HOXA10.

Circ_0010235 Could Upregulate HOXA10 by Sponging miR-588 in NSCLC Cells

The regulation of circ_0010235 by HOXA10 was analyzed by western blotting. The silencing of circ_0010235 downregulated the expression of HOXA10, which was counterbalanced by anti-miR-588 in A549 and H1299 cells (Figure 8a and 8a). This confirms that circ_0010235 regulates HOXA10 by targeting miR-588.

DISCUSSION

Previous studies have reported that circ_0010235 plays an oncogenic role in NSCLC by targeting the miRNA/mRNA axis^{7,8}. In this study, for the first time, we identified that circ_0010235 accelerated tumor cell behaviors and reduced the radiation sensitivity in NSCLC through miR-588/HOXA10 axis.

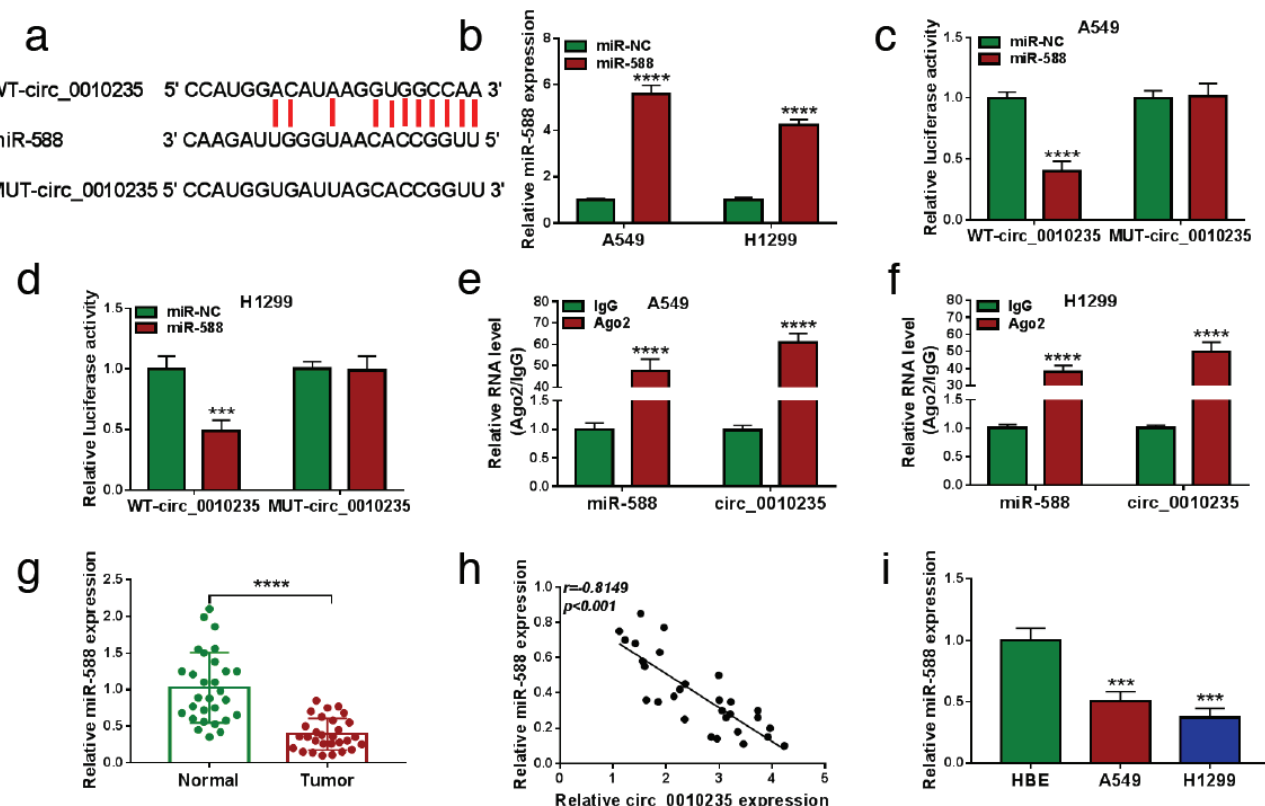


FIG. 4. Circ_0010235 interacts with miR-588. (a) The binding sites between circ_0010235 and miR-588 were predicted through starbase. (b) RT-qPCR was used to assess the transfection efficiency of miR-588 in A549 and H1299 cells. (c-f) The dual-luciferase reporter (c-d) and RIP (e-f) assays were used to validate the binding between circ_0010235 and miR-588. (g) RT-qPCR was applied to measure the expression of miR-588 in NSCLC tissues. (h) Pearson's correlation was used to analyze the linear relationship between circ_0010235 and miR-588. (i) RT-qPCR was applied to quantify the level of miR-588 in A549 and H1299 cells. ***P < 0.001, ****P < 0.0001.

CircRNAs have high structural stability and tissue specificity and these characteristics provide the important foundation for circRNAs as cancer biomarkers¹⁸. For example, circ_001888 was abnormally expressed in gastric cancer and used as a probable diagnostic biomarker¹⁹. Circ_0010235 was identified as a closed-loop circRNA through the stability analysis using RNase R treatment and through the structure analysis using Oligo (dT)₁₈ primers. In this study, a significant upregulation of circ_0010235 was detected in the NSCLC tissues and cells, implying that circ_0010235 might be a diagnostic indicator for NSCLC.

Several studies have elucidated the regulatory roles of circRNAs in the development of cancers. Liu et al.²⁰ found that proliferation, migratory capacity, and invasiveness were restrained by the silencing of circFOXM1 in prostate cancer cells. In addition, CircDIDO1 overexpression repressed the malignant phenotypes of gastric cancer cells²¹ and circ_0011385 upregulation

contributed to the biological development of cervical cancer.²² Our experimental data show that the silencing of circ_0010235 triggered the repression of cell growth, invasion, and migration, as well as the stimulation of apoptosis. In addition, circRNAs could regulate tumor sensitivity to radiation treatment. Moreover, previous studies demonstrated that CircRNA_100367 promoted radioresistance in esophageal squamous cell carcinoma and that circ_0055625 suppressed radiosensitivity in colon cancer^{23,24}. Herein, we found that circ_0010235 siRNA sensitized the NSCLC cells to radiation. Furthermore, the animal studies also confirmed that the downregulation of circ_0010235 expression resulted in tumor growth inhibition and radiosensitivity restoration in vivo. The knockdown of circ_0010235 might be used to prevent tumor progression and inhibit radiation resistance in clinical patients.

Different circRNA/miRNA axes have been found in the regulation of cancer. For instance, circ_0000523 modulated proliferation

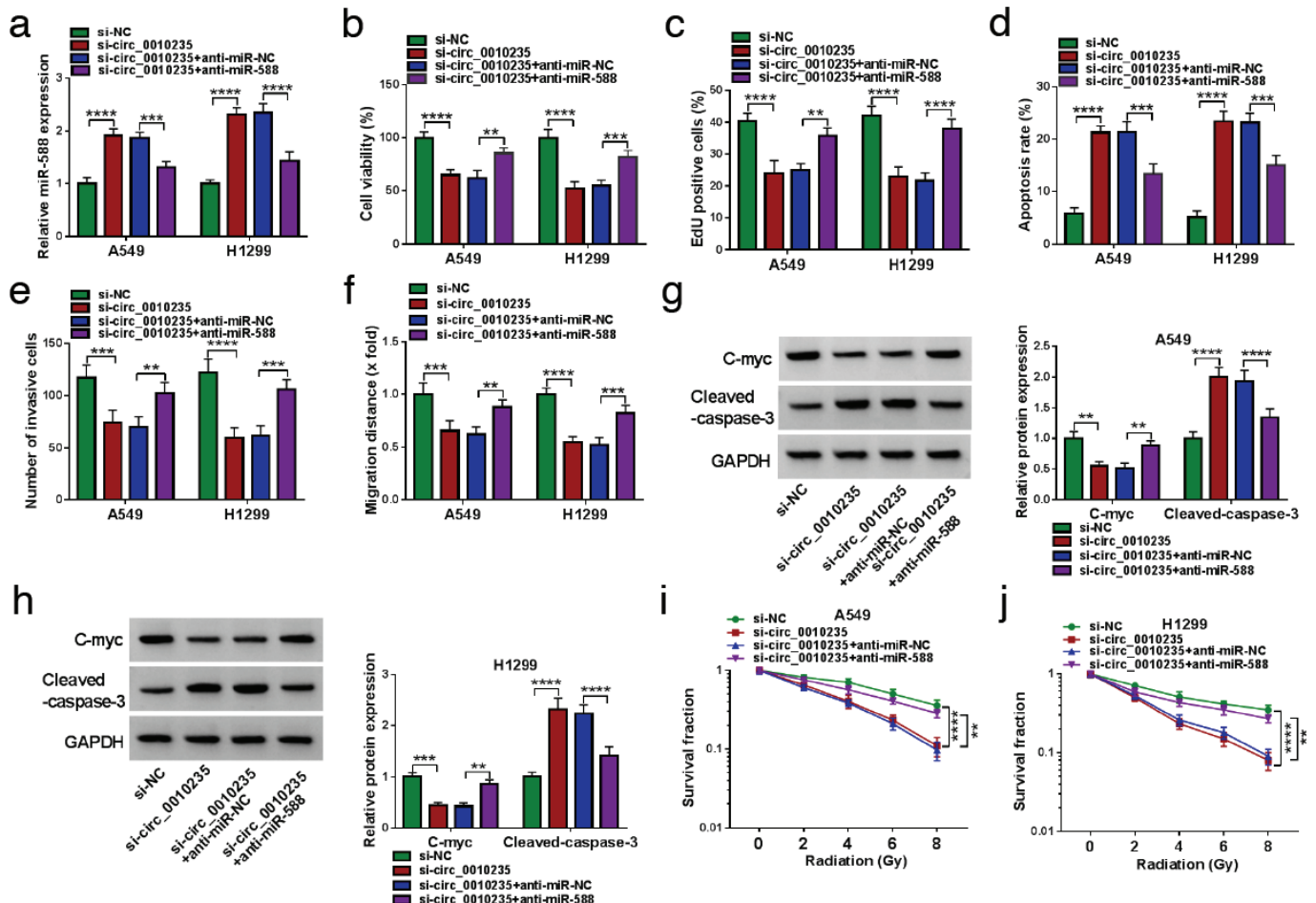


FIG. 5. MiR-588 inhibition counters the regulatory function of si-circ_0010235 in NSCLC cells. The transfection of si-NC, si-circ_0010235, si-circ_0010235+anti-miR-NC, or si-circ_0010235+anti-miR-588 was conducted in A549 and H1299 cells. (a) The quantification of circ_0010235 was performed via RT-qPCR. (B-C) Cell viability (b) and proliferation (c) was determined via the CCK-8 and Edu assays, respectively. (d) Cell apoptosis was determined by flow cytometry. (e-f) The assessment of invasion (e) and migration (f) was performed via the transwell and wound healing assays, respectively. (g-h) The detection of c-myc and cleaved-caspase-3 was performed by western blotting. (i-j) The analysis of cell survival was done by the colony formation assay after radiation treatment. **P < 0.01, ***P < 0.001, ****P < 0.0001.

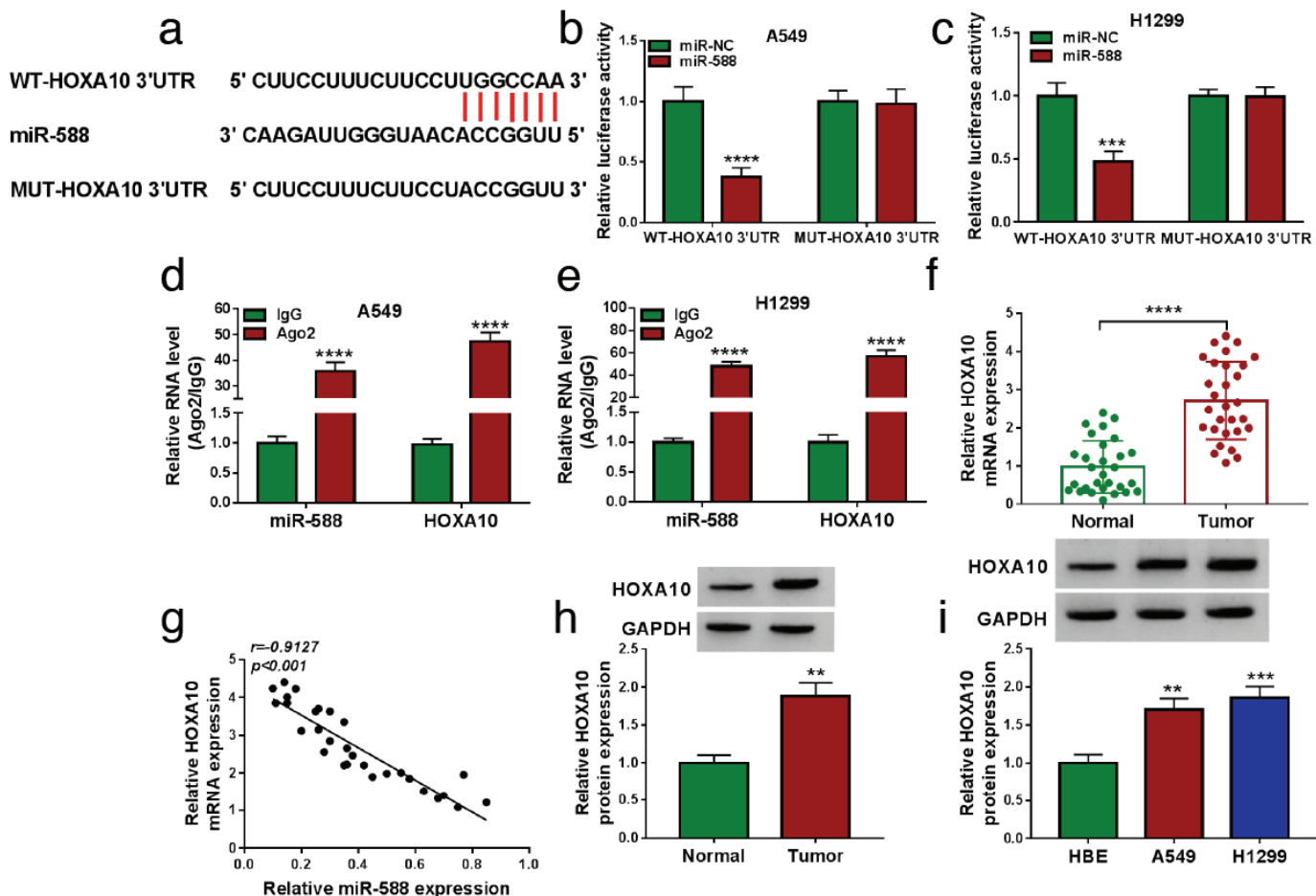


FIG. 6. HOXA10 is a downstream target of miR-588. (a) Starbase was used for target prediction between HOXA10 and miR-588. (b-e) The combination between HOXA10 and miR-588 was conducted through the dual-luciferase reporter (b-c) and RIP assays (d-e). (f) HOXA10 mRNA expression was examined via RT-qPCR. (g) The relationship between HOXA10 and miR-588 expression was analyzed by Pearson's correlation. (h-i) The protein level of HOXA10 was measured via western blotting. ** $P < 0.01$, *** $P < 0.001$, **** $P < 0.0001$.

and apoptosis by sponging miR-31 in colorectal cancer cells.²⁵ CircADAMTS13 induced the sponging of miR-484, which restrained the proliferation of hepatocellular carcinoma.²⁶ Also, the circ_0010235 sequence harbored the miR-588 binding sites and could bind to miR-588 in NSCLC cells. Furthermore, our reverted results demonstrated that the function of circ_0010235 was ascribed to the sponging effect of miR-588 in NSCLC cells.

In addition, miR-588 exerted tumor-suppressive effects by targeting EIF5A2 in gastric cancer and downregulating GRN in NSCLC.^{9,27} In this study, miR-588 inhibited cancer behaviors but elevated radiation sensitivity by targeting HOXA10. More importantly,

HOXA10 expression was regulated by circ_0010235 via miR-588 sponging in NSCLC. The circRNA/miRNA/mRNA regulatory networks have participated in the NSCLC progression.²⁸⁻³⁰ Therefore, circ_0010235 was involved in the functional regulation of oncogenesis and radiosensitivity via the miR-588/HOXA10 axis in NSCLC cells.

We report that circ_0010235 drove malignant progression and radiation resistance in NSCLC by upregulating HOXA10 expression via sponging miR-588 (Figure 9). This study has shown a special molecular mechanism in the pathogenesis and radioresistance of NSCLC.

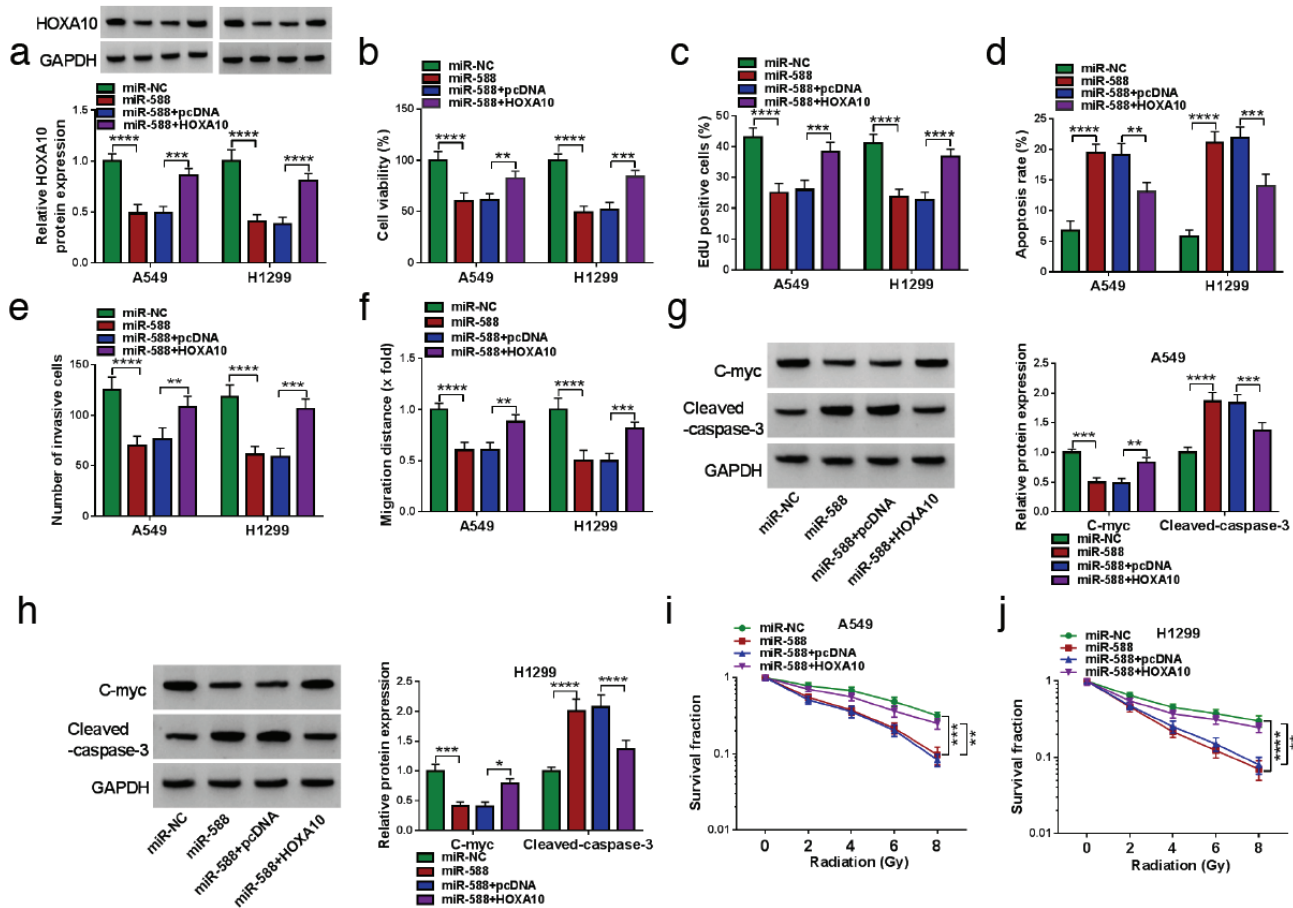


FIG. 7. MiR-588 acts as a tumor inhibitor and radiation sensitizer by targeting HOXA10. The transfection of miR-NC, miR-588, miR-588+pcDNA, and miR-588+HOXA10 was performed in A549 and H1299 cells. (a) Western blotting was used for the analysis of HOXA10 protein expression. (b-c) The CCK-8 and EdU assays were used to determine cell viability (b) and proliferation (c), respectively. (d) Flow cytometry was used for apoptosis examination. (e-f) The transwell and wound healing assays were applied for the assessment of invasion (e) and migration (f), respectively. (g-h) Western blotting was applied for the detection of c-myc and cleaved-caspase-3. (i-j) The colony formation assay was used for survival analysis after cells were treated with radiation. *P < 0.05, **P < 0.01, ***P < 0.001, ****P < 0.0001.

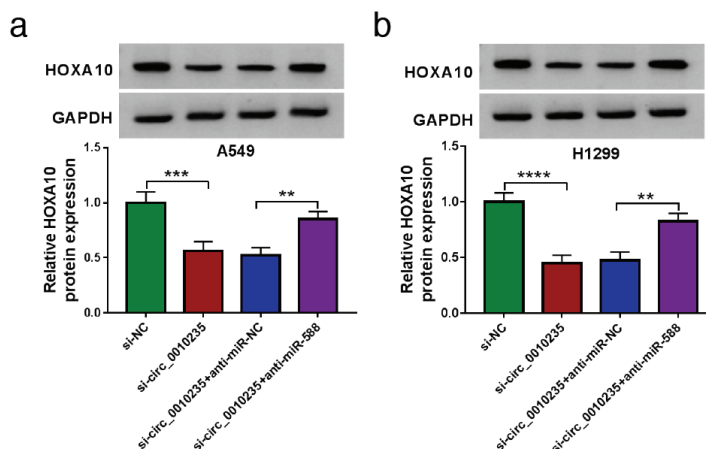


FIG. 8. Circ_0010235 could upregulate HOXA10 by sponging miR-588 in NSCLC cells. (a) Western blotting conducted to determine the protein expression of HOXA10 in the si-NC, si-circ_0010235, si-circ_0010235+anti-miR-NC, or si-circ_0010235+anti-miR-588 transfection group. **P < 0.01, ***P < 0.001, ****P < 0.0001.

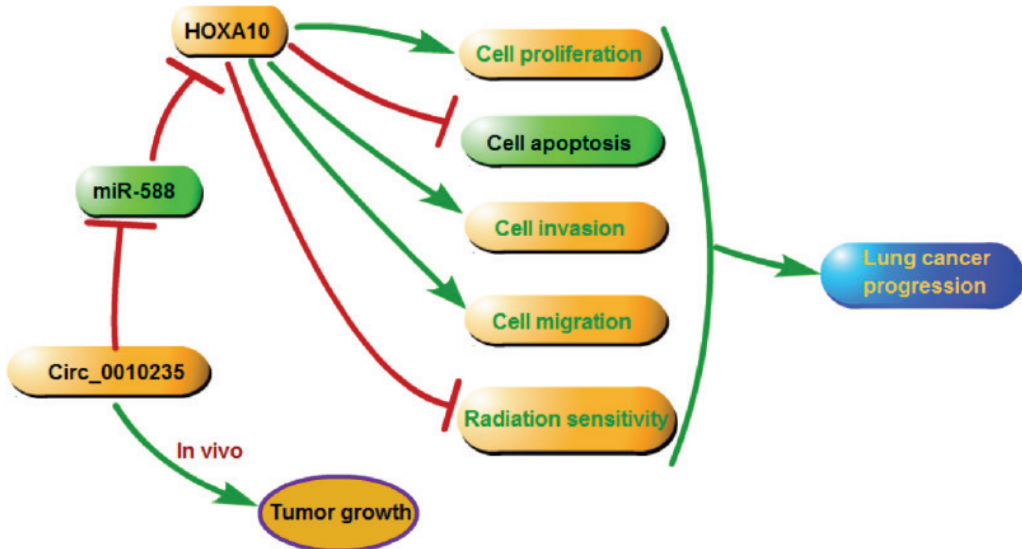


FIG. 9. Graphical abstract of circ_0010235/miR-588/HOXA10 axis in NSCLC progression and radioresistance.

Ethics Committee Approval: This study was approved by the Ethics Committee of Xiangyang No.1 People's Hospital. The clinicopathologic features of patients with NSCLC and their association with circ_0010235 expression are contained in Table 1.

Data Sharing Statement: The raw data supporting the conclusions of this article will be made available by the authors, without undue reservation.

Author Contributions: Concept- C.C.; Design- C.C.; Data Collection or Processing- W.Y.; Analysis or Interpretation- W.Y.; Literature Search- H.Z.; Writing- S.Y.

Conflict of Interest: No conflict of interest was declared by the authors.

Funding: The authors declared that this study received no financial support.

REFERENCES

- Zhao Y, Liu Y, Li S, et al. Role of lung and gut microbiota on lung cancer pathogenesis. *J Cancer Res Clin Oncol.* 2021;147:2177-2186. [\[CrossRef\]](#)
- Yousefi M, Ghaffari P, Nosrati R, et al. Prognostic and therapeutic significance of circulating tumor cells in patients with lung cancer. *Cell Oncol (Dordr).* 2020;43:31-49. [\[CrossRef\]](#)
- Xie S, Wu Z, Qi Y, Wu B, Zhu X. The metastasizing mechanisms of lung cancer: Recent advances and therapeutic challenges. *Biomed Pharmacother.* 2021;138:111450. [\[CrossRef\]](#)
- Wang C, Tan S, Li J, Liu WR, Peng Y, Li W. CircRNAs in lung cancer - Biogenesis, function and clinical implication. *Cancer Lett.* 2020;492:106-115. [\[CrossRef\]](#)
- Tang S, Li S, Liu T, et al. MicroRNAs: Emerging oncogenic and tumor-suppressive regulators, biomarkers and therapeutic targets in lung cancer. *Cancer Lett.* 2021;502:71-83. [\[CrossRef\]](#)
- Wang X, Li H, Lu Y, Cheng L. Circular RNAs in Human Cancer. *Front Oncol.* 2021;10:577118. [\[CrossRef\]](#)
- Zhang F, Cheng R, Li P, Lu C, Zhang G. Hsa_circ_0010235 functions as an oncogenic drive in non-small cell lung cancer by modulating miR-433-3p/TIPRL axis. *Cancer Cell Int.* 2021;21:73. [\[CrossRef\]](#)
- Zhu Y, Ma C, Lv A, Kou C. Circular RNA circ_0010235 sponges miR-338-3p to play oncogenic role in proliferation, migration and invasion of non-small-cell lung cancer cells through modulating KIF2A. *Ann Med.* 2021;53:693-706. [\[CrossRef\]](#)
- Qian L, Lin L, Du Y, Hao X, Zhao Y, Liu X. MicroRNA-588 suppresses tumor cell migration and invasion by targeting GRN in lung squamous cell carcinoma. *Mol Med Rep.* 2016;14:3021-3028. [\[CrossRef\]](#)
- Song C, Han Y, Luo H, et al. HOXA10 induces BCL2 expression, inhibits apoptosis, and promotes cell proliferation in gastric cancer. *Cancer Med.* 2019;8:5651-5661. [\[CrossRef\]](#)
- Yuan Y, Sun S, Jiao N, Shu Y, Zhang Y. Upregulation of HOXA10 Protein Expression Predicts Poor Prognosis for Colorectal Cancer. *Genet Test Mol Biomarkers.* 2018;22:390-397. [\[CrossRef\]](#)
- Cui YP, Xie M, Pan WX, Zhang ZY, Li WF. HOXA10 promotes the development of bladder cancer through regulating FOSL1. *Eur Rev Med Pharmacol Sci.* 2020;24:2945-2954. [\[CrossRef\]](#)
- Ma T, Hu Y, Guo Y, Yan B. Tumor-Promoting Activity of Long Noncoding RNA LINC00466 in Lung Adenocarcinoma via miR-144-Regulated HOXA10 Axis. *Am J Pathol.* 2019;189:2154-2170. [\[CrossRef\]](#)
- He WW, Ma HT, Guo X, Wu WM, Gao EJ, Zhao YH. lncRNA SNHG3 accelerates the proliferation and invasion of non-small cell lung cancer by downregulating miR-340-5p. *J Biol Regul Homeost Agents.* 2020;34:2017-2027. [\[CrossRef\]](#)
- Yang QS, Li B, Xu G, et al. Long noncoding RNA LINC00483/microRNA-144 regulates radiosensitivity and epithelial-mesenchymal transition in lung adenocarcinoma by interacting with HOXA10. *J Cell Physiol.* 2019;234:11805-11821. [\[CrossRef\]](#)
- Hou J, Wang Y, Zhang H, Hu Y, Xin X, Li X. Silencing of LINC00461 enhances radiosensitivity of lung adenocarcinoma cells by down-regulating HOXA10 via microRNA-195. *J Cell Mol Med.* 2020;24:2879-2890. [\[CrossRef\]](#)
- Livak KJ, Schmittgen TD. Analysis of relative gene expression data using real-time quantitative PCR and the 2(-Delta Delta C(T)) Method. *Methods.* 2001;25:402-408. [\[CrossRef\]](#)
- Drula R, Braicu C, Harangiu A, et al. Critical function of circular RNAs in lung cancer. *Wiley Interdiscip Rev RNA.* 2020;11:e1592. [\[CrossRef\]](#)
- Shi P, Song H, Ding X. Reduced expression of circRNA hsa_circ_001888 in gastric cancer and its clinical significance. *J Clin Lab Anal.* 2021;35:e23953. [\[CrossRef\]](#)
- Liu GX, Zheng T, Zhang Y, Hao P. CircFOXM1 silencing represses cell proliferation, migration and invasion by regulating miR-515-5p/ADAM10 axis in prostate cancer. *Anticancer Drugs.* 2022;33:e573-e583. [\[CrossRef\]](#)
- Zhang Y, Jiang J, Zhang J, et al. CircDIDO1 inhibits gastric cancer progression by encoding a novel DIDO1-529aa protein and regulating PRDX2 protein stability. *Mol Cancer.* 2021;20:101. [\[CrossRef\]](#)
- Xu AL, Wang WS, Zhao MY, Sun JN, Chen XR, Hou JQ. Circular RNA circ_0011385 promotes cervical cancer progression through competitively binding to miR-149-5p

- and up-regulating SOX4 expression. *Kaohsiung J Med Sci.* 2021;37:1058-1068. [\[CrossRef\]](#)
23. Liu J, Xue N, Guo Y, et al. CircRNA_100367 regulated the radiation sensitivity of esophageal squamous cell carcinomas through miR-217/Wnt3 pathway. *Aging (Albany NY).* 2019;11:12412-12427. [\[CrossRef\]](#)
24. Gao C, Zhang Y, Tian Y, et al. Circ_0055625 knockdown inhibits tumorigenesis and improves radiosensitivity by regulating miR-338-3p/MSI1 axis in colon cancer. *World J Surg Oncol.* 2021;19:131. [\[CrossRef\]](#)
25. Jin Y, Yu LL, Zhang B, Liu CF, Chen Y. Circular RNA hsa_circ_0000523 regulates the proliferation and apoptosis of colorectal cancer cells as miRNA sponge. *Braz J Med Biol Res.* 2018;51:e7811. [\[CrossRef\]](#)
26. Qiu L, Huang Y, Li Z, et al. Circular RNA profiling identifies circADAMTS13 as a miR-484 sponge which suppresses cell proliferation in hepatocellular carcinoma. *Mol Oncol.* 2019;13:441-455. [\[CrossRef\]](#)
27. Zhou X, Xu M, Guo Y, et al. MicroRNA-588 regulates invasion, migration and epithelial-mesenchymal transition via targeting EIF5A2 pathway in gastric cancer. *Cancer Manag Res.* 2018;10:5187-5197. [\[CrossRef\]](#)
28. Liu W, Ma W, Yuan Y, Zhang Y, Sun S. Circular RNA hsa_circRNA_103809 promotes lung cancer progression via facilitating ZNF121-dependent MYC expression by sequestering miR-4302. *Biochem Biophys Res Commun.* 2018;500:846-851. [\[CrossRef\]](#)
29. Zhang P, Xue XF, Ling XY, et al. CircRNA_010763 promotes growth and invasion of lung cancer through serving as a molecular sponge of miR-715 to induce c-Myc expression. *Eur Rev Med Pharmacol Sci.* 2020;24:7310-7319. [\[CrossRef\]](#)
30. Wan J, Hao L, Zheng X, Li Z. Circular RNA circ_0020123 promotes non-small cell lung cancer progression by acting as a ceRNA for miR-488-3p to regulate ADAM9 expression. *Biochem Biophys Res Commun.* 2019;515:303-309. [\[CrossRef\]](#)